Limit analysis on RC-structures by a multi-yield-criteria numerical approach

Aurora Angela Pisano, Paolo Fuschi, Dario De Domenico

Abstract The present study proposes a multi-yield-criteria limit analysis numerical procedure for the prediction of peak loads and failure modes of reinforced concrete (RC) elements. The proposed procedure, which is a generalization of a previous one recently presented by the authors, is hereafter applied to structural elements reinforced either with traditional steel bars and stirrups or with fiber reinforced polymer (FRP) sheets used as strengthening system. The procedure allows to take into account the actual behaviour, at a state of incipient collapse, of steel, FRP and concrete by a finite element (FE) based plasticity approach where concrete is governed by a Menétrey-Willam-type yield criterion, FRP reinforcement obey to a Tsai-Wu-type yield criterion and steel reinforcement follow the von Mises yield criterion. To check the effectiveness and reliability of the numerically detected peak loads and failure modes a comparison with experimental laboratory findings, available in literature for large-scale specimens, is presented.

1 Introduction

The design of concrete structures reinforced either with classical steel bars or with innovative FRP bars, as well as the strengthening or the rehabilitation of existing steel RC structures through externally bonded FRP sheets or strips, are subjects of great interest in the field of civil engineering. This interest is witnessed by a huge amount of analytical and experimental research studies proposed in the relevant literature in the last decades (see e.g. [2, 9]). Among the several methods already developed and the different aspects anlayzed, from an engineering point of view, it is of utmost importance the knowledge at ultimate (collapse) state of the load carrying capacity of such structures. This task can indeed be pursued, within

Aurora Angela Pisano, Paolo Fuschi, Dario De Domenico
University *Mediterranea* of Reggio Calabria Dept. PAU - via Melissari, I-89124 Reggio Calabria, Italy. e-mail: aurora.pisano@unirc.it;cpaolo.fuschi@unirc.it;cdario.dedomenico@unirc.it.

a plasticity-based approach, using Limit Analysis. Although plain concrete is not a ductile material, experimental studies have shown that the presence of longitudinal web or stirrups reinforcement, as well as of FRP laminates, render the global behaviour of RC structural elements quite ductile so justifying the applicability of approaches based on plasticity theory [3, 5, 10]. It is the realm of the so called *direct methods* which often utilise finite element method (FEM) in conjunction with optimization algorithms such as linear [27] and nonlinear programming [11, 14, 28]. These approaches indeed do not allow the treatment of post elastic phenomena that may arise in concrete structures, such as localization, fracture, damage, creep etc., and that can be faced by coupling plasticity with fracture or damage mechanics theories within step-by-step analyses (see e.g. [12, 15, 30]); however, they can give information on the behaviour at limit (collapse) states of such structures, so resulting very useful for design purposes. In this context it has to be framed the present study.

The promoted approach belongs to a wider research program started by the authors in the context of laminates of FRP [18, 19, 21] and extended to RC structures with reference to a Menétrey-Willam (M-W)-type yield criterion with cap in compression [8, 20, 22]. In the latter studies, two limit analysis methods, namely the Linear Matching Method, LMM, [24], and the Elastic Compensation Method, ECM, [16], have been applied under the hypothesis that reinforcement behave as indefinitely elastic. This assumption has inevitably produced some drawbacks. In particular only those structures whose behaviour at incipient collapse is dominated by crushing of concrete, that is the case of the so-called over-reinforced structures, can be appropriately analyzed, while for under-reinforced structures, where reinforcement often attain their limit capabilities, the methods result less accurate. To overcome this limitation and improve the overall analysis of the RC structural elements at collapse enhancements of the methods have been presented in [23]. The present study proposes a further advanced version of the methods that considers possible yielding of steel bars as well as collapse of FRP sheets. To this purpose the paper proposes a three yield criteria limit analysis formulation in which concrete is governed by a Menétrey-Willam-type yield criterion with cap in compression, steel reinforcement follow the von Mises yield criterion and FRP reinforcement obey to a Tsai-Wu-type yield criterion. This allows to predict the peak loads of those RC structures in which steel and/or FRP reinforcement play an important role in the behaviour exhibited at a state of incipient collapse. The effectiveness of the proposed approach is shown by comparison of the obtained numerical predictions with the experimental findings on steel reinforced beams strengthened in flexure using GFRP sheets.

It is worth noting that the promoted procedure is of general (wider) applicability, the only essential requisite being the strict convexity of the yield criteria assumed for the constituent materials.

The paper is organized as follows: after this introductory section, Section 2 gives the principles of the LMM and ECM employed in the limit analysis procedure and this with reference to a *generic, strictly convex, yield criterion*; Section 3 recalls few analytical expressions of the Menétrey-Willam-type yield criterion enriched with a cap in compression, of the Tsai-Wu-type yield criterion and of the von Mises yield

criterion, just to set up the constitutive relations; Section 4 and Section 5 particularize the LMM and ECM to the three yield criteria here considered; Section 6 gives the results obtained by analyzing large scale RC beams strengthened with FRP sheet and compares these results with the available experimental tests; finally Section 7 draws some conclusions.

2 Limit analysis: basic concepts and numerical issues

Limit analysis allows the direct evaluation of the load bearing capacity of a structure or of a structural element. In its classical formulation the theory of limit analysis refers to perfectly plastic structures, made of standard materials, and it is based on a lower and an upper bound theorem ([6, 26]). The bound theorems allow the exact determination of the (unique) load value that will cause collapse.

The upper bound theorem states that an upper bound, say P_{UB}, to the collapse load multiplier for a given body of volume V is given by:

$$P_{UB} = \frac{\int_V \sigma_j^Y \, \dot{\varepsilon}_j^c \, \mathrm{d}V}{\int_{\partial V_t} \bar{p}_i \, \dot{u}_i^c \, \mathrm{d}(\partial V)}, \tag{1}$$

where: $\dot{\varepsilon}_j^c = \dot{\lambda} \, \partial f / \partial \sigma_j$ are the components of the strain rate at collapse having the direction of the outward normal to the yield surface $f(\sigma_j) = 0$ (with $\dot{\lambda} > 0$ a scalar multiplier); σ_j^Y are the stresses at yield associated to the given compatible strain rates $\dot{\varepsilon}_j^c$; $\dot{u}_i^c$ are the related displacement rates. Moreover, $\bar{p}_i$ are the surface force components of the reference load vector $\bar{\mathbf{p}}$ acting on the external portion ∂V_t of the body surface. For simplicity, only surface forces are considered. The set $(\dot{\varepsilon}_j^c, \dot{u}_i^c)$ defines a collapse mechanism.

On the other hand, the lower bound theorem states that if at every point within V exists a stress field $\widetilde{\sigma}_j$ which satisfies the condition $f(\widetilde{\sigma}_j) \leq 0$ and in equilibrium with the applied load $P\bar{\mathbf{p}}$ for a value of P, say P_{LB}, then P_{LB} is a lower bound to the collapse limit load multiplier.

The two assertions above, as known, lead to two classical approaches of limit analysis, namely: the kinematic and the static one. If the loads produced by their application are equal to each other, circumstance verifiable only for standard materials, then they equal the collapse load. As a matter of fact, the success of limit analysis approaches has been determined also by the possibility to apply the theory, with due attention, outside the realm of perfect plasticity so allowing the study of structures made of non standard materials. The non standard limit analysis theory is based on the two Radenkovic's fundamental theorems which can be summarized as: "every value of the limit load for a non standard body is located between two fixed boundaries defined by the values of the limit loads computed considering the body made by two standard materials whose yield surfaces are one outer, the other inner, to that of the nonstandard material." Obviously, within a nonstandard Radenkovic's

approach only a range of collapse load multiplier values can be located between two computed bounds, the uniqueness of the limit load being missing.

The nonstandard approach will be followed hereafter, the main constituent materials of the addressed structural elements being indeed modelled by plasticity-based criteria of non associative type. The assumed yield surface playing the double role of outer and inner "standard" surfaces mentioned before. The promoted approach is based on sequences of FE elastic analyses as well as on the use, in concomitance, of two distinct limit analysis numerical methods, i.e.: the LMM which follows the kinematic approach of limit analysis theory [18, 20, 24] and the ECM which is grounded on the static approach [16, 21, 22]. For sake of brevity, the LMM and the ECM will be discussed with reference to a *generic, strictly convex, yield surface*, namely an ellipsoid in principal stress space. To this concern it is worth noting that the applicability of the whole approach is independent from the assumed stress field representation as will appear more clear in Sections 4 and 5 where the adopted yield criteria will be explicited.

2.1 Upper bound evaluation via LMM

The LMM, firstly theorized by Ponter and Carter [24] for von Mises materials and then extended to more complex materials in [20–22], is an iterative procedure involving *one* sequence of *linear analyses*. The linear analyses are carried on the structure made, by hypothesis, of a *linear viscous fictitious material* with *spatially varying moduli*, D_I (I ranging over the elastic constants entering the considered material), and *imposed initial stresses*, $\bar{\sigma}_j$ (j ranging over the considered (needed) stress components). The adjective *fictitious* highlights the property of the material endowed with elastic parameters which may assume different values at different points; the latter being Gauss points (GPs) in a FE discrete model of the structure.
An easy understanding of the method can be achieved by looking at its geometrical interpretation sketched in Fig.1. At the current iteration, say at the $(k-1)th$ FE-analysis, the fictitious structure (i.e. the structure under study with its real geometry, boundary and loading conditions but made of fictitious material) is analyzed under loads $P^{(k-1)}\bar{p}_i$, with $P^{(k-1)}$ load multiplier and $\bar{p}_i$ assigned reference loads.
The fictitious linear solutions computed, at each Gauss Point of the FE mesh, can be represented by a point $\mathbb{P}_L^{(k-1)}$ lying on the complementary dissipation rate equipotential surface referred to the fictitious viscous material, say $W^{(k-1)}(\sigma_j^{\ell(k-1)}, D_I^{(k-1)}, \bar{\sigma}_j^{(k-1)}) = \bar{W}^{(k-1)}$, whose geometrical dimensions and center position depend on the fictitious values $D_I^{(k-1)}$ and $\bar{\sigma}_j^{(k-1)}$ fixed at the current GP. The point $\mathbb{P}_L^{(k-1)}$ with its coordinates, say $\sigma_j^{\ell(k-1)}$ in the chosen principal stress space, shown in the sketch of Fig.1, represents the fictitious solution in terms of stresses while the outward normal at $\mathbb{P}_L^{(k-1)}$, say the normal of components $\dot{\varepsilon}_j^{\ell(k-1)}$, represents the fictitious solution in terms of linear viscous strain rates. At this stage the fictitious moduli and

initial stresses are *modified* so that $\mathbb{P}_L^{(k-1)}$ is brought onto the yield surface of the real constitutive material the analyzed structure is made with. The latter surface is here presented by the ellipsoidal shaded surface of Fig.1. Namely $\mathbb{P}_L^{(k-1)}$ is brought to identify with point $\mathbb{P}_M^{(k-1)}$, having the same outward normal of $\mathbb{P}_L^{(k-1)}$ but lying on the real material yield surface.

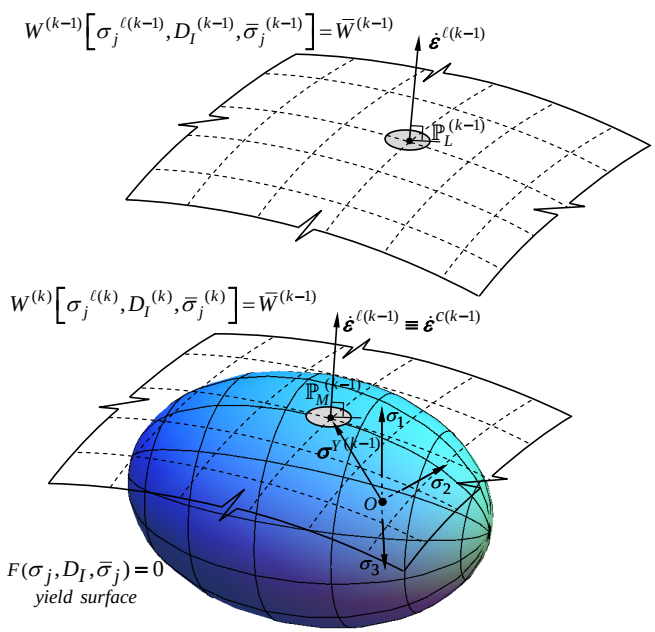

Fig. 1 Geometrical sketch, in the principal stress space, of the matching procedure, from iteration $(k-1)$ to (k), at the current GP within the current element.

The fictitious solution in terms of strain rates, namely $\dot{\varepsilon}_j^{\ell(k-1)} \equiv \dot{\varepsilon}_j^{c(k-1)}$, where the apex c stands for "at collapse", as well as the stress coordinates of $\mathbb{P}_M^{(k-1)}$, say the stresses at yield $\boldsymbol{\sigma}_j^{Y(k-1)}$, give all the information pertaining to a *state of incipient collapse built at the current GP*. In particular, the fictitious strain rates $\dot{\varepsilon}_j^{\ell(k-1)} \equiv \dot{\varepsilon}_j^{c(k-1)}$, with the associated displacement rates $\dot{u}_j^{\ell(k-1)} \equiv \dot{u}_j^{c(k-1)}$, define a *collapse mechanism*. The related stresses $\boldsymbol{\sigma}_j^{Y(k-1)}$ are the pertinent *stresses at yield*. Indeed, for the formal analogy existing between the linear viscous problem and the linear elastic problem the strain rates $\dot{\varepsilon}_j^{\ell(k-1)}$ can be evaluated as linear *elastic* strain rates, viewing $W^{(k-1)} = const$ as the complementary energy equipotential surface of the fictitious material. While the described modification of $D_I^{(k-1)}$ and $\bar{\sigma}_j^{(k-1)}$ implies

that the "modified" $W^{(k)}(\boldsymbol{\sigma}_j^{\ell(k)}, D_I^{(k)}, \bar{\boldsymbol{\sigma}}_j^{(k)}) = \bar{W}^{(k-1)}$ *matches* the yield surface at point $\mathbb{P}_M^{(k-1)}$, see again Fig.1.

Operatively, the matching procedure performed at the current GP starts with the search of the stress point $\mathbb{P}_M^{(k-1)}$ on the yield surface having an assigned strain rate $\dot{\boldsymbol{\varepsilon}}^{\ell(k-1)} \equiv \dot{\boldsymbol{\varepsilon}}^{c(k-1)}$ as outward normal.

It is worth noting that if the yield surface is strictly convex such point $\mathbb{P}_M^{(k-1)}$ is uniquely determined by the given normal $\dot{\boldsymbol{\varepsilon}}^{\ell(k-1)}$. If this normal belongs to a cone of normals pertaining to a vertex (nonsmooth corner) if any, of the yield surface, point $\mathbb{P}_M^{(k-1)}$ simply identifies with this vertex.
If the expounded rationale is repeated at all GPs of the mesh, a collapse mechanism, $(\dot{\varepsilon}_j^{c(k-1)}, \dot{u}_i^{c(k-1)})$ with the related stresses at yield, $\boldsymbol{\sigma}_j^{Y(k-1)}$ can be defined for the whole structure and, by Eq. (1), an upper bound value to the collapse load multiplier, say $P_{UB}^{(k)}$, can be evaluated at current $(k-1)th$ FE elastic analysis. However, the above stress at yield, computed through the matching, do not meet the equilibrium conditions with the acting loads $P^{(k-1)}\bar{p}_i$ and the procedure is carried on iteratively until the difference between two subsequent P_{UB} values is less than a fixed tolerance. Convergence requires that the $W^{(k)} = \bar{W}^{(k-1)}$ matches the yield surface at $\mathbb{P}_M^{(k-1)}$ and otherwise lies outside the yield surface (see [25]). In the following the LMM is applied simultaneously to concrete, FRP and steel reinforcement.

2.2 Lower bound evaluation via ECM

The ECM conceived by Mackenzie and Boyle [16] with reference to steel and then modified to deal with more complex materials in Pisano et al. [18, 22] is aimed to construct an admissible stress field, suitable for the evaluation of a P_{LB} , in the spirit of the static approach of limit analysis. Also the ECM is an iterative procedure involving *many* sequences of linear elastic FE-based analyses, in which highly loaded regions of the structure are systematically weakened by reduction of the elastic moduli and this in order to simulate a *stress redistribution* arising within the structure before attaining its limit strength threshold. Also in this case the procedure can be more easily explained by means of a geometrical sketch as the one given in Fig.2 with reference to a generic yield surface $F(\boldsymbol{\sigma}_j, D_I, \bar{\boldsymbol{\sigma}}_j) = 0$. The ECM starts with a first sequence, say $s = 1$, of FE elastic analyses, carried on the structure endowed with the proper (real) material elastic parameters and suffering applied initial loads $P_D^{(s)}\,\bar{p}_i = P_D^{(1)}\,\bar{p}_i$. At the current iteration, say at the $(k-1)th$ FE analysis, the elastic stress solution is computed at the GPs of the mesh. Such values, averaged within the current element #e, allow to define a solution "at element level", which, as shown in the sketch of Fig.2, locates in the principal stress space a stress point, say $\mathbb{P}_{\#e}^{e(k-1)}$. $\mathbb{P}_{\#e}^{Y(k-1)}$ denotes the corresponding stress point at yield (i.e. lying on the yield surface) measured on the direction $\overrightarrow{O\mathbb{P}_{\#e}^{e}}/|\overrightarrow{O\mathbb{P}_{\#e}^{e}}|$. In the figure are reported other stress points, representing the average stress elastic solution within the ele-

ments #1, #2, ..., #e, ..., #n. If the elastic solution at the #e-th element is such that $|\overrightarrow{O\mathbb{P}}^{e}_{\#e}|^{(k-1)} > |\overrightarrow{O\mathbb{P}}^{Y}_{\#e}|^{(k-1)}$ then the element's Young modulus is reduced according to the formula:

$$E^{(k)}_{\#e} = E^{(k-1)}_{\#e} \left[\frac{|\overrightarrow{O\mathbb{P}}^{Y}_{\#e}|^{(k-1)}}{|\overrightarrow{O\mathbb{P}}^{e}_{\#e}|^{(k-1)}} \right]^2 \tag{2}$$

where the square of the updating ratio, within the square bracket, is used to increase the convergence rate.

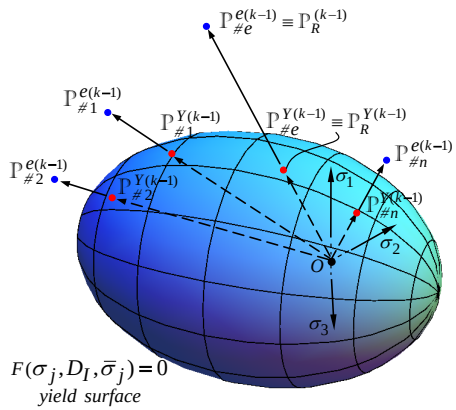

Fig. 2 Geometrical sketch, in the principal stress space, of the ECM at current iteration $(k-1)$ of the current sequence s. Stress points representing the elastic solution at elements #1, #2, ..., #e, ..., #n; with $\mathbb{P}^{(k-1)}_{R}$ denoting the "maximum stress" among all the elements.

After the above modulus variation, the *maximum stress value* has to be detected in the *whole FE mesh*, namely the value corresponding to the stress point farthest away from the yield surface, say $\mathbb{P}^{(k-1)}_{R}$ in the sketch of Fig.2. If $|\overrightarrow{O\mathbb{P}}_{R}|^{(k-1)}$ is greater than $|\overrightarrow{O\mathbb{P}}^{Y}_{R}|^{(k-1)}$ (as drawn Fig.2) a *new* FE analysis is performed within the current sequence trying to *re-distribute* the stresses within the structure; and this by keeping fixed the applied loads but with the updated $E^{(k)}_{\#e}$ values given by Eq.(2). The iterations are carried on, inside the given sequence, until all the stress points just reach or are below their corresponding yield values, which means that an admissible stress field has been built. Increased values of loads are then considered in the subsequent sequences of analyses, each one with an increased value of $P^{(s)}_{D}$, till further load increase does not allow the stress point $\mathbb{P}^{(k-1)}_{R}$ to be brought below yield by the re-distribution procedure. A P_{LB} load multiplier can then be evaluated at *last admis-*

sible stress field attained for a maximum acting load $P_D^{(s)}\bar{p}_i$, say at $s = S$, and at last FE analysis, say at $k = K$, as:

$$P_{LB} = |\overrightarrow{O\mathbb{P}}_R^Y|^{(K)} \frac{P_D^{(S)}}{|\overrightarrow{O\mathbb{P}}_R|^{(K)}}. \tag{3}$$

3 Yield-criteria for RC structures

As outlined in the introductory section, this study is focused on concrete elements reinforced with steel bars and externally strengthened with FRP sheets. The main goal is indeed to apply the limit analysis approach, described in Section 2, to the yield criteria assumed for the constituent materials of the analyzed RC elements, namely: concrete, FRP laminates and steel. The main constitutive assumptions are given next.

Concrete is assumed as an isotropic nonstandard material obeying a plasticity model derived from the Menétrey-Willam [17](M-W) failure criterion; this criterion is defined by the following expression:

$$F(\xi,\rho,\theta) = \left[\sqrt{1.5}\frac{\rho}{f_c'}\right]^2 + m\left[\frac{\rho}{\sqrt{6}f_c'}\, r(\theta,e) + \frac{\xi}{\sqrt{3}f_c'}\right] - 1 = 0; \tag{4}$$

where:

$$r(\theta,e) = \frac{4\left(1-e^2\right)\cos^2\theta + (2e-1)^2}{2\left(1-e^2\right)\cos\theta + (2e-1)\left[4\left(1-e^2\right)\cos^2\theta + 5e^2 - 4e\right]^{1/2}};$$

$$m := 3\,\frac{f_c'^2 - f_t'^2}{f_c' f_t'}\,\frac{e}{e+1}. \tag{5}$$

Equation (4) is given in terms of three stress invariants ξ,ρ,θ known as the Haigh Westergaard (H-W) coordinates; m is the friction parameter of the material depending, as shown in Eq.(5), on the compressive strength f_c', the tensile strength f_t' as well as on the eccentricity parameter e, whose value governs the convexity and smoothness of the elliptic function $r(\theta,e)$. The eccentricity e describes the out-of-roundness of M-W deviatoric trace and it strongly influences the biaxial compressive strength of concrete. To limit the concrete strength in high hydrostatic compression regime, a cap, closing in compression the surface defined by Eq.(4), is adopted. This cap, formulated in the H-W coordinates, can be given the shape:

$$\rho^{CAP}(\xi,\theta) = -\frac{\rho^{MW}(\xi_a,\theta)}{(\xi_a-\xi_b)^2}\left[\xi^2 - 2\xi_a(\xi-\xi_b) - \xi_b^2\right], \text{ with } \left\{\begin{matrix}\xi_b \le \xi \le \xi_a \\ 0 \le \theta \le \frac{\pi}{3}\end{matrix}\right.; \tag{6}$$

where $\rho^{MW}(\xi,\theta)$ is the explicit form of the parabolic meridian of the M-W surface that, looking at Eq. (7), can be given by:

$$\rho^{MW}(\xi,\theta)=\frac{1}{2a}\left\{-b(\theta)+\left[b^2(\theta)-4ac(\xi)\right]^{1/2}\right\},\ \text{with}\ \left\{\begin{array}{c}\xi_a\le\xi\le\xi_v\\ 0\le\theta\le\frac{\pi}{3}\end{array}\right.; \quad (7)$$

and where:

$$a=\frac{1.5}{\left(f_c'\right)^2};\quad b(\theta)=\frac{m}{\sqrt{6}f_c'}r(\theta,e);\quad c(\xi)=\frac{m}{\sqrt{3}f_c'}\xi-1. \quad (8)$$

The values ξ_a, ξ_b and ξ_v entering Eqs.(6) and (7) locate the cap position and can be detected experimentally.
It is worth noting that the Menétrey-Willam surface equipped with a cap in compression is strictly convex and smooth, except for the vertices on the hydrostatic axis, and it is hereafter assumed as yield criterion for concrete. A realistic representation of concrete requires to take into account the dilatancy so a non-associated flow rule is also postulated.

The FRP laminate, the strengthening sheets are made with, are assumed as a composite, orthotropic, nonstandard material obeying a plasticity model derived from the Tsai-Wu failure criterion [29]. By denoting with 1 and 2 the principal directions of orthotropy in plane stress case as well as indicating, as usual in this context, $\sigma_6\equiv\tau_{12}$, the adopted Tsai-Wu-type yield surface is given by:

$$F(\sigma_1,\sigma_2,\sigma_6)=F_{11}\,\sigma_1^2+F_{22}\,\sigma_2^2+F_{66}\,\sigma_6^2+2\,F_{12}\,\sigma_1\sigma_2+F_1\,\sigma_1+F_2\,\sigma_2-1=0, \quad (9)$$

where:

$$\begin{aligned}&F_1:=\frac{1}{X_t}+\frac{1}{X_c};\quad F_2:=\frac{1}{Y_t}+\frac{1}{Y_c};\quad F_{11}:=-\frac{1}{X_t\,X_c};\\ &F_{22}:=-\frac{1}{Y_t\,Y_c};\quad F_{66}:=\frac{1}{S^2};\quad F_{12}:=-\frac{1}{2}\sqrt{F_{11}F_{22}};\end{aligned} \quad (10)$$

with: X_t, X_c the longitudinal tensile and compressive strengths respectively; Y_t, Y_c the transverse tensile and compressive strengths respectively and S the longitudinal shear strength. In Eq.(10) the compressive strengths X_c and Y_c have to be considered intrinsically negative. Equation (9) represents in the space $\sigma_1,\sigma_2,\sigma_6$ an ellipsoid whose major axis lies on the $\sigma_6=0$ plane and it is rotated by an anticlockwise angle of 45^0 with respect to the σ_1 axis. This surface is hereafter assumed as yield criterion for the FRP composite reinforcement. Also in this case a non-associated flow rule is postulated.

Finally, steel follows the von Mises yield criterion which is one of the most popular criteria applied to describe the behaviour of perfectly plastic ductile materials. For a generic, multi-axial, loading condition and considering that $\rho^2=2J_2$ (with J_2

second stress deviatoric invariant) the von Mises yield surface, being σ_y the yield strength, is expressed in the form:

$$F(\rho) = \frac{3}{2}\rho^2 - \sigma_y^2 = 0, \tag{11}$$

that, in the case of uniaxial stress condition, like the one recorded in the reinforcement bars, simply reduces to $\sigma_1 = \sigma_y$, being σ_1 the first principal stress, measured along the bar longitudinal direction. As known, in the principal stress space the von Mises yield surface of Eq.(11) is represented by a cylinder, indefinite along the hydrostatic axis, circumstance that does not satisfy the required condition of strict convexity. However the limit analysis procedure will be pursued on the deviatoric plane where the von Mises criterion is a circle of radius $\rho_y = \sqrt{\frac{2}{3}}\sigma_y$.

4 Three-yield-criteria LMM

The LMM procedure presented in Section 2.1, with reference to a generic strictly convex yield surface, can be now easily specified for concrete, FRP and steel. To this aim, taking into account the assumed yield criteria, it will be sufficient to specify the apposite expressions of the complementary energy equipotential surface $W^{(k-1)}(\sigma_j^{\ell\,(k-1)}, D_I^{(k-1)}, \bar{\sigma}_j^{(k-1)}) = \bar{W}^{(k-1)}$ that has to be consistent with the yield criterion in use. Looking at concrete, governed by the M-W-type yield surface by Eqs.(4)-(8), the pertinent complementary energy equipotential surface, in the Haigh-Westergaard coordinate, depends on the bulk modulus K, on the shear modulus G as well as on initial stresses, $\bar{\xi}$ and $\bar{\rho}$. With reference to the rationale of Section 2.1, then, referring to Fig.1, the elastic moduli D_I identify with G and K, while $\bar{\sigma}_j$ correspond to $\bar{\xi}$ and $\bar{\rho}$. At the current iteration $(k-1)$ of the LMM procedure and at the current GP within the mesh, the right complementary energy functional can be given the shape:

$$W^{(k-1)}(\xi,\rho) = \frac{\left(\xi - \bar{\xi}^{\,(k-1)}\right)^2}{6K^{(k-1)}} + \frac{\left(\rho - \bar{\rho}^{\,(k-1)}\right)^2}{4G^{(k-1)}}. \tag{12}$$

Equation (12), written as $W^{(k-1)} = \bar{W}^{(k-1)}$ represents, in the principal stress space, a *prolate spheroid* having semi axes proportional to the elastic parameters $(G^{(k-1)}, K^{(k-1)})$ and coordinates of the center depending on the initial stresses $(\bar{\xi}^{\,(k-1)}, \bar{\rho}^{\,(k-1)})$.

The LMM acts updating the elastic moduli and the initial stresses of Eq.(12) in such a way that the spheroid is modified in shape and position till matching is realized on the M-W-type surface at the stress point of given outward normal. In this context the normal components are the *volumetric* and *deviatoric* strain rates of the fictitious linear solution, namely: $\dot{\varepsilon}_v^{\ell\,(k-1)} \equiv \dot{\varepsilon}_v^{c\,(k-1)}$ and $\dot{\varepsilon}_d^{\ell\,(k-1)} \equiv \dot{\varepsilon}_d^{c\,(k-1)}$. The above matching point $\mathbb{P}_M^{(k-1)}$ $(\xi^{Y\,(k-1)}, \rho^{Y\,(k-1)})$ gives, with its H-W coordinates, the associated

stresses at yield. A nonlinear system of 5 equations provides the searched matching point. The quite complex geometrical problem associated to the LMM applied to M-W-type yield surface has been deeply discussed in a recent paper by the authors [20].

For the FRP strengthening sheets, at a current iteration $(k-1)$ and at a current GP, the complementary energy functional consistent with the T-W-type yield criterion, given by Eqs.(9), (10), can instead be written as:

$$W\left(\sigma_j, E_j^{(k-1)}, \nu_{12}^{(k-1)}, \bar{\sigma}_j^{(k-1)}\right) = \frac{1}{2}\left[\frac{\sigma_1^2}{E_1^{(k-1)}} + \frac{\sigma_2^2}{E_2^{(k-1)}} + \frac{\sigma_6^2}{E_6^{(k-1)}} - 2\,\nu_{12}^{(k-1)}\,\frac{\sigma_1\,\sigma_2}{E_2^{(k-1)}} + \right.$$
$$-2\left(\frac{\bar{\sigma}_1^{(k-1)}}{E_1^{(k-1)}} - \nu_{12}^{(k-1)}\,\frac{\bar{\sigma}_2^{(k-1)}}{E_2^{(k-1)}}\right)\sigma_1 - 2\left(\frac{\bar{\sigma}_2^{(k-1)}}{E_2^{(k-1)}} - \nu_{12}^{(k-1)}\,\frac{\bar{\sigma}_1{}^{(k-1)}}{E_2^{(k-1)}}\right)\sigma_2$$
$$\left. -2\,\frac{\bar{\sigma}_6^{(k-1)}}{E_6^{(k-1)}}\sigma_6 + \frac{\bar{\sigma}_1^{(k-1)^2}}{E_1^{(k-1)}} + \frac{\bar{\sigma}_2^{(k-1)^2}}{E_2^{(k-1)}} + \frac{\bar{\sigma}_6^{(k-1)^2}}{E_6^{(k-1)}} - 2\,\nu_{12}^{(k-1)}\,\frac{\bar{\sigma}_1^{(k-1)}\,\bar{\sigma}_2^{(k-1)}}{E_2^{(k-1)}}\right], \quad (13)$$

where E_6 is the shear modulus G_{12}. The surface obtainable by Eq.(13) represents in the stress space (σ_1, σ_2, σ_6) an ellipsoid whose semi axes amplitude depend on the elastic moduli, while its center position depends on the initial stresses. Referring again to the sketch of Fig.1, that can be easily redrawn with reference to the stress components σ_1, σ_2, σ_6, the elastic parameter D_I identify with E_1, E_2, E_6, ν_{12}, while $\bar{\sigma}_j$ corresponds to $\bar{\sigma}_1$, $\bar{\sigma}_2$, $\bar{\sigma}_6$. The ellipsoid $W^{(k-1)} = \bar{W}^{(k-1)}$ is in all similar to the Tsai-Wu-type yield surface and this simplifies the matching procedure. By appropriately choosing the initial values of the elastic parameters and initial stresses of the fictitious material, the complementary energy surface may indeed result *homothetic* to the T-W-type surface and the matching procedure can be realized just by a rescaling of the complementary energy surface. To this aim it is sufficient to rescale by *only one* scalar coefficient the elastic parameters E_j, which govern the amplitude of the axes of $W^{(k-1)} = \bar{W}^{(k-1)}$, through the updating formula:

$$E_j^{(k)} = E_j^{(k-1)}\,(\Lambda^{(k-1)})^2, \quad (j = 1, 2, 6) \quad (14)$$

being the scalar coefficient $\Lambda^{(k-1)}$ the homothetic ratio between the two ellipsoids, [18, 19]. In this case homothety implies that $W = \bar{W}$, at matching, simply *coincides* with the yield surface. The points $\mathbb{P}_L^{(k-1)}$ and $\mathbb{P}_M^{(k-1)}$ not only have the same normal of components $\dot{\varepsilon}_j^{c\,(k-1)}$, with $j = 1,2,6$, (as required by matching) but they belong, since the beginning, to the same straight line passing through the stress space origin. Eventually, at matching, the coordinates of $\mathbb{P}_M^{(k-1)}$, namely $\sigma_j^{Y\,(k-1)}$ with $j = 1,2,6$ give the pertinent stresses at yield.

The application of the LMM results even more simple with reference to the von Mises yield criterion. Nevertheless, the sketch of Fig.1 becomes meaningless, the

von Mises yield surface being in the principal stress space a cylinder indefinite along its axis coincident with the hydrostatic axis. The procedure can indeed be carried on with reference to the deviatoric plane where the essential requisite of strict convexity is recovered, the von Mises surface being a circle. Looking at the geometrical sketch of Fig.3(a), under the hypothesis of incompressible fictitious material the pertinent complementary energy potential functional consistent with a von Mises material, at a current iteration $(k-1)$, can be written as:

$$W(\rho, E^{(k-1)}) = \frac{3\rho^2}{4E^{(k-1)}} \tag{15}$$

which, if written in the shape $W^{(k-1)} = \bar{W}^{(k-1)}$, represents a circle concentric to the von Mises one. With reference to Fig.3(a), the linear fictitious solution at a current iteration, $(k-1)$, and at the current GP can be represented by the deviatoric stress invariant, point $\mathbb{Q}_L^{(k-1)}$ $(|O\mathbb{Q}_L^{(k-1)}| \equiv \rho^{(k-1)})$, having outward normal the deviatoric strain rate $\dot{\varepsilon}_d{}^{(k-1)}$.
To find the corresponding matching point $\mathbb{Q}_M^{(k-1)}$ it is sufficient to move along the radius $\overrightarrow{O\mathbb{Q}_L}^{(k-1)}$ that is to re-scale the complementary energy surface by modifying the Young modulus $E^{(k-1)}$ with the updating formula:

$$E^{(k)} = E^{(k-1)} \frac{\rho_y}{\rho^{(k-1)}} \tag{16}$$

that brings $W^{(k-1)} = \bar{W}^{(k-1)}$ to coincide with the von Mises deviatoric circle of radius ρ_y. In the case of uniaxial stress condition, as the one detected in the steel bars, Eq.(16) is further simplified, i.e.:

$$E^{(k)} = E^{(k-1)} \frac{\sigma_y}{\sigma_1^{(k-1)}}. \tag{17}$$

The key idea of the present approach is now achievable: the LMM is applied simultaneously to *all* the FEs of the discrete model of the RC structure, i.e. to each GP of each element. The proper yield condition and matching procedure will be used at the GPs of the FEs describing concrete, FRP sheets and steel bars.
When, at current iteration and *for each* GP of the FE mesh the stresses at yield, the corresponding strain rates at collapse, together with the associated displacement rates at collapse, are known, it is possible to compute an upper bound multiplier, say $P_{UB}^{(k)}$, by applying Eq.(1) that particularizes as follows:

$$P_{UB}^{(k)} = \frac{\int_V (\xi^{Y\,(k-1)}\,\dot{\varepsilon}_v^{c\,(k-1)} + \rho^{Y\,(k-1)}\,\dot{\varepsilon}_d^{c\,(k-1)} + \sigma_j^{Y\,(k-1)}\,\dot{\varepsilon}_j^{c\,(k-1)} + \rho_y\,\dot{\varepsilon}_d^{c\,(k-1)})\mathrm{d}V}{\int_{\partial V_t} \bar{p}_i\,\dot{u}_i^{c\,(k-1)}\,\mathrm{d}(\partial V)}. \tag{18}$$

As said, the iterative procedure is carried on until the difference between two subsequent P_{UB} values is less than a fixed tolerance.

5 Three-yield-criteria ECM

Following the same rationale of the previous section, the ECM, presented in its general formulation in Section 2.2, is also applied to the whole structure. The admissible stress field for a given maximum applicable load has to be detected with respect to each of constituent materials yield surface.

With reference to concrete and FRP sheets, the point $\mathbb{P}_{\#e}^{e(k-1)}$ of Fig.2 has to be simply interpreted with the pertinent coordinates, namely: ($\xi_{\#e}^{e(k-1)}$, $\rho_{\#e}^{e(k-1)}$, $\theta_{\#e}^{e(k-1)}$) in the Haigh-Westergaard coordinates when dealing with M-W-type yield surface or ($\sigma_{\#e_1}^{e(k-1)}$, $\sigma_{\#e_2}^{e(k-1)}$, $\sigma_{\#e_6}^{e(k-1)}$) when working on FRP sheets within the (σ_1, σ_2, σ_6) stress space. $\mathbb{P}_{\#e}^{Y(k-1)}$ denotes the corresponding stress point on the yield surface, measured on the direction $\overrightarrow{O\mathbb{P}}_{\#e}^{e}/|\overrightarrow{O\mathbb{P}}_{\#e}^{e}|$ and the reduction formula given by Eq.(2) holds true and it has to be applied if the elastic solution at the #e-th element is such that $|\overrightarrow{O\mathbb{P}}_{\#e}^{e}|^{(k-1)} > |\overrightarrow{O\mathbb{P}}_{\#e}^{Y}|^{(k-1)}$.
In particular, assuming that the concrete Poisson ratio ν remains constant, the updating of the Young modulus by Eq.(2) is equivalent to modify the bulk modulus $K_{\#e}^{(k-1)}$ and shear modulus $G_{\#e}^{(k-1)}$ by the same reducing factor. When dealing with FRP reinforcement the reduction is applied instead to the three element's Young moduli of #e, namely to $E_{\#e_j}^{(k)}$, $j = 1,2,6$.

With reference to steel, at the current iteration $(k-1)$, the deviatoric stress invariant $\rho_{\#e}^{(k-1)}$ evaluated within the steel bar elements #1,#2,..., #e,..., #n, can be represented as in Fig.3(b). As said, in the elements where $\rho_{\#e}^{(k-1)}$ is greater than ρ_y the elastic modulus must be modified (reduced). This goal can be achieved by varying the elastic modulus as in Eq.(16). It is worth to remark that the "modulus variation" realized by Eq.(16) possesses, in this case, a completely different meaning. When it is applied within the LMM, the above variation (reduction or increse), is driven by a fixed strain rate and, as said, it is oriented to build a collapse mechanism. On the other hand when such modulus variation is applied within the ECM it is always a reduction necessary to bring a not admissible stress onto the yield surface so realizing a stress redistribution oriented to build an admissible stress field. It has also to be noted that the LMM acts on all the GPs of the FE mesh. All the GPs are viewed as possible sites where a mechanism might arise. The confinement of the plasticized zone is obtained only at convergence. On the contrary, the ECM acts only on the elements characterized by stress quantities greater than the yielding ones in the attempt to mimic a stress redistribution within the structure. Also in this case, it has been numerically experienced that the convergence rate increases if the square of the updating ratio, $\rho_y/\rho_{\#e}^{(k-1)}$, is used so the updating formula becomes:

$$E_{\#e}^{(k)} = E_{\#e}^{(k-1)} \left[\frac{\rho_y}{\rho_{\#e}^{(k-1)}} \right]^2 . \tag{19}$$

Within the current sequence, after the described moduli redistribution on concrete, FRP laminates and steel bars, the three *maximum stress values* have to be detected in the *whole FE mesh*. Precisely, the three stress points farthest away from the yield surfaces considered, say $\mathbb{P}_R^{(k-1)}$ for concrete or FRP and $\rho_R^{(k-1)}$ for steel bars.

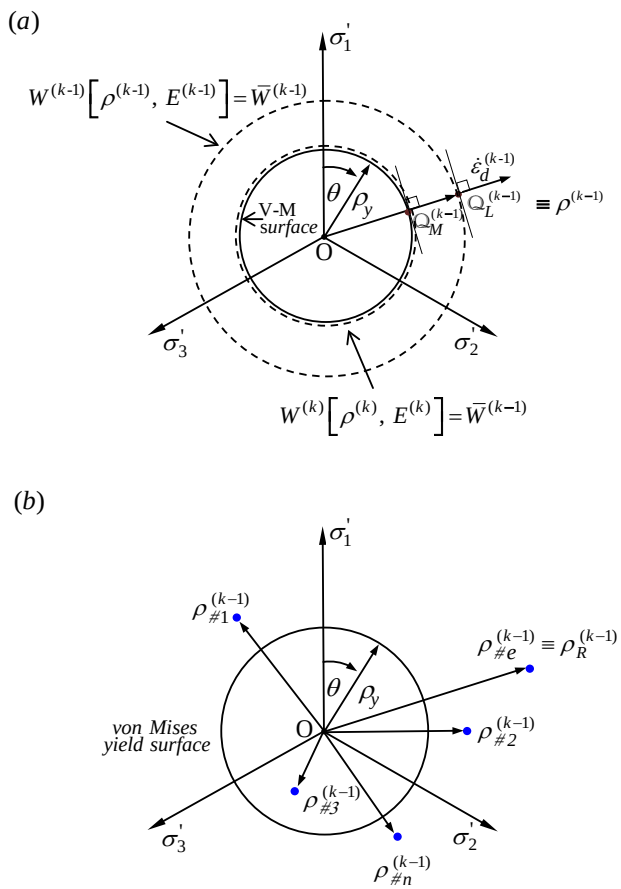

Fig. 3 Geometrical sketch of the limit analysis procedure in the deviatoric plane for steel bars: (a) matching procedure from iteration $(k-1)$ to (k) performed at current GP of current bar elements; (b) stress points measured within the steel bar elements $\#1, \#2, \#3, \ldots, \#e, \ldots, \#n$ to apply ECM, $\rho_R^{(k-1)}$ denoting the "maximum stress" among the bar elements.

Referring again to Fig.2 and Fig.3(b) if $|\overrightarrow{O\mathbb{P}_R}|^{(k-1)}$ is greater than $|\overrightarrow{O\mathbb{P}_R^Y}|^{(k-1)}$ or $\rho_R^{(k-1)}$ is greater than ρ_y a new FE analysis is performed within the current sequence keeping fixed the applied load but with the updated $E_{\#e}^{(k)}$ given by Eqs.(2)

and (19). The iterations are carried on, inside the given sequence, until all the stress points just reach or are below their corresponding yield values, which means that an admissible stress field has been built. Increased values of loads are then considered in the subsequent sequences, each one with an increased value of $P_D^{(s)}$, till further load increase does not allow the maximum stresses to be brought below yield by redistribution. A P_{LB} load multiplier can then be evaluated at *last admissible stress field* attained for a *maximum acting load* $P_D^{(s)}\bar{p}_i$, say at $s = S$, and at last FE analysis, say at $k = K$, as the minimum between the three values:

$$P_{LB} = \min\left\{ \left[|\overrightarrow{O\mathbb{P}_R^Y}|^{(K)} \frac{P_D^{(S)}}{|\overrightarrow{O\mathbb{P}_R}|^{(K)}} \right]_{CONCR} ; \left[|\overrightarrow{O\mathbb{P}_R^Y}|^{(K)} \frac{P_D^{(S)}}{|\overrightarrow{O\mathbb{P}_R}|^{(K)}} \right]_{FRP} ; \rho_y \frac{P_D^{(S)}}{\rho_R^{(K)}} \right\}. \tag{20}$$

6 Applications

The main goal of the following applications is to verify the reliability of the expounded three-yield-criteria limit analysis numerical procedure in predicting the limit state (peak load and failure mechanism) of structural RC elements strengthened by FRP sheets. Experimental findings on large scale specimens, taken from the relevant literature, have been numerically reproduced and the obtained results have been compared with those given by the laboratory tests.

In all the numerical analyses a perfect bonding between steel bars and concrete as well as between FRP sheets and concrete has been assumed. Reference is made to the experimental works of Almusallam and Al-Salloum [1] who thested, up to failure, steel reinforced concrete beams strengthened with Glass FRP (GFRP) sheets. Indeed, the above quoted paper faces a number of experimental tests, carried out to investigate the effects of the GFRP strengthening on the flexural capacity and central deflection of the beams, so that the experimental campaign considers beams with and without GFRP reinforcements. Only some of the available experimental results are then taken into consideration, namely those in which the sheets of GFRP are present. In particular, using the same label of Almusallam and Al-Salloum [1], the analyzed beams are: GB2, GB4 and GB6.

The beams are simply supported and subjected to four-point bending test through two line loads $P\bar{p}/2$ placed at the same distance with respect to the mid-span. For all the considered specimens, P denotes the load multiplier, while $\bar{p}$ denotes the line reference load whose resultant is assumed equal to 100kN. Figure 4(a) shows the mechanical scheme used for beams together with all the geometrical details. Only half specimen is modeled due to symmetry with respect to the longitudinal direction. The beams are reinforced with different arrangement of internal steel bars and stirrups, and strengthened with different arrangement of GFRP sheets as reported in Figures 4(b). Furthermore, the relevant material properties for concrete and GFRP

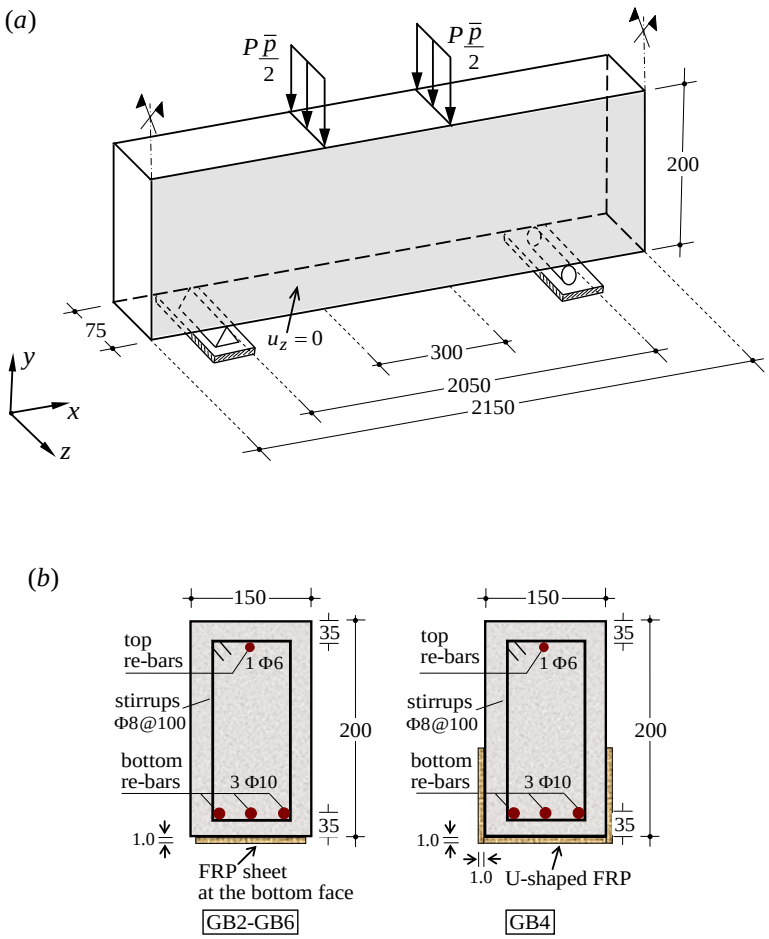

Fig. 4 Mechanical model of the analyzed simply-supported beams GB2, GB4, GB6: (a) geometry, loading and boundary conditions; (b) cross section geometry with reinforcement arrangement (after Almusallam and Al-Salloum [1]); all the dimensions are in mm.

reinforcement are given in Tables 1 and 2 respectively, while, for what concerns steel a Young modulus of $200GPa$ and a yield strength σ_y of $537MPa$ have been assumed for all specimens.

It has to be noted that in Table 1 the uniaxial tensile strength value has been computed as $f_t^{'} = 0.33\sqrt{f_c^{'}}$ as suggested by Bresler and Scordelis [4], and the elastic concrete modulus has been assumed $E_c = 22(f_c^{'}/10)^{0.3}$ according to Eurocode 2. Moreover, for what concerns the choices related to the adopted concrete constitutive model, the value of the eccentricity parameter e of the M-W-type yield surface

has been evaluated by the expression $e = \left[2 + f_t^{'}/f_c^{'}\right] \Big/ \left[4 - f_t^{'}/f_c^{'}\right]$, the $f_t^{'}/f_c^{'}$ being assumed as a measure of the material brittleness. Finally, the value of ξ_v can be expressed as $\xi_v = \sqrt{3} f_c^{'} \big/ m$, while ξ_a and ξ_b have been set equal to $\xi_a = 0.7923\, f_c^{'}$ and $\xi_b = 1.8964\, f_c^{'}$ as suggested by Li and Crouch [13][2010].

Table 1 Mechanical parameters of concrete for the analyzed beams.

specimen label	*concrete properties*		
	$f_c^{'}$ *(MPa)*	$f_t^{'}$ *(MPa)*	E_c *(GPa)*
GB2	36.00	1.98	32.31
GB4	36.60	2.00	32.47
GB6	33.80	1.92	31.70

Concerning the numerical model, it is worth noting that in both LMM and ECM the elastic analyses can be carried out by *any* commercial FE code. In the following applications the ADINA code has been used while a Fortran main program has been used to drive the FE analyses within the sequences. The elastic analyses performed within the LMM and ECM have been carried out using FE meshes of 3D-solid 8-nodes elements with 2x2x2 GPs per element for modeling concrete, 2-D-solid plane stress 4-nodes elements for modeling GFRP laminates and 2-nodes, 1-GP, truss elements for modeling steel bars and stirrups. To set up the FE model of each analyzed specimen a preliminary mesh sensitivity study, to assure an accurate FE elastic solution, has been performed. More precisely, the number of 3D-solid elements is 504, that of truss elements is 246, while the number of 2D-solid elements ranges from 80 to 160.

Table 2 Mechanical parameters of FRP laminae of the strengthening sheets.

FRP lamina moduli				*FRP lamina strengths*				
E_1 *(GPa)*	E_2 *(GPa)*	G_{12} *(GPa)*	ν_{12}	X_t *(MPa)*	X_c *(MPa)*	Y_t *(MPa)*	Y_c *(MPa)*	S *(MPa)*
30.0	30.0	3.80	0.28	600	600	600	600	89

The obtained numerical results are reported in Tables 3 in which, for the three analyzed specimens, are given: the peak load multiplier experimentally detected P_{EXP}; the predictions in terms of upper and lower bound values, P_{UB} and P_{LB}, and the relative errors (in %), $Err(P_{UB})$ and $Err(P_{LB})$, computed as the difference between

the numerical detected values and the experimental ones over the experimental one.

Table 3 Peak load multipliers for the analyzed RC beams: values experimentally detected, P_{EXP}; values of the upper and lower bounds, P_{UB} and P_{LB}; relative errors, Err (P_{UB}) and Err (P_{LB}).

Specimen label	*Peak load multipliers*			*Relative error %*	
	P_{EXP}	P_{UB}	P_{LB}	Err (P_{UB})	Err (P_{LB})
GB2	0.562	0.596	0.498	6.05	-11.39
GB4	0.587	0.649	0.550	10.56	-6.30
GB6	0.635	0.671	0.580	5.67	-8.66

With the adopted definition of the relative errors, the upper bound values are expected to have a positive relative error, while the lower bound values are expected to have a negative relative error. The inspection of the numerical findings highlights the very good prediction obtained with the proposed three-yield-criteria limit analysis approach. In order to have a more immediate perception of the quality of the numerical predictions, the data of Table 3 are drawn in Fig.5 as histograms. Other quite encouraging results have been obtained on FRP strengthened RC beams and slabs (see e.g. [7]), but are not reported here for lack of space.

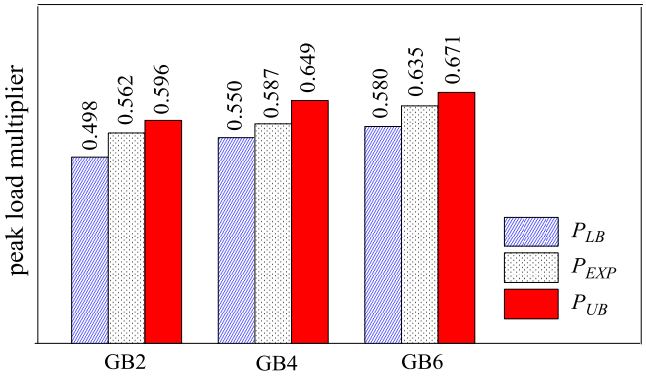

Fig. 5 Comparison between numerical and experimental peak load multipliers for the analyzed beams.

The LMM gives also some hints on the type of failure mechanisms. Such a prediction in fact is given by the possibility to point out the plastic zone (portions of the FE-mesh where the collapse mechanism has been eventually located) at “last

converged solution" of the LMM. Just to show one of the analysed cases, the plots of the principal (compressive) strain rates $\dot{\varepsilon}_3^c$ within RC concrete elements and of the principal strain rates $\dot{\varepsilon}_1^c$ within GFRP elements have been considered for beam GB4, at convergence. Plots are shown in Figs.6(a, b). By inspection of Fig.6 it is possible to observe a plasticized zone, corresponding to a plastic hinge spread at beam center. This zone appears reasonably narrow and located where the damaged zones have been actually experimentally detected, as confirmed by the photograph given in Fig.6(c) concerning beam GB4 at failure. It is worth to mention that the band plots of Figs.6(a, b) provides only qualitative information of the failure mechanisms, but they can be anyway useful to localize critical zones or weaker members within larger structural systems.

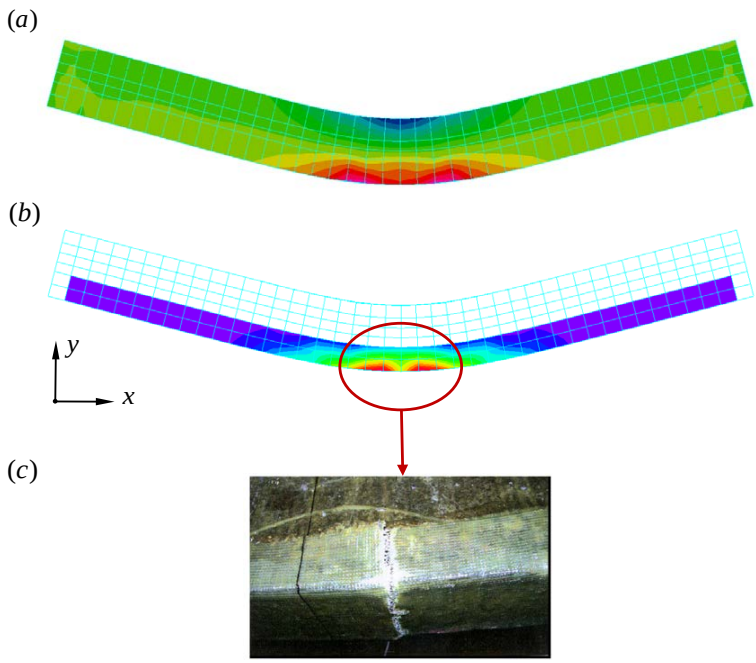

Fig. 6 Prediction of the failure mechanism for the beam GB4. Band plots of principal strain rates, in the deformed configuration, at last converged solution of the LMM. (a) RC elements; (b) FRP laminate elements; (c) photograph at midspan of beam GB6 at failure (after Almusallam and Al-Salloum [1]).

7 Concluding remarks

A multi-yield-criteria limit analysis numerical procedure for the prediction of peak loads and failure modes of steel-reinforced concrete elements strengthened with FRP laminates has been proposed. The behavior at ultimate state of the constituents, namely: concrete, FRP sheets and steel bars has been taken into account by a numerical procedure that involves, in concomitance, a Menétrey Willam-type yield criterion with cap in compression for concrete, a Tsai Wu-type yield criterion for the FRP strengthening reinforcement and the von Mises yield criterion for steel bars. The lack of associativity, postulated for concrete, to deal with its dilatancy, and for the FRP sheets, due to their compositive nature, has led to search for an upper and a lower bound to the peak load multiplier of the whole RC structural element. The former has been pursued by the LMM, the latter by the ECM. Both methods have been applied simultaneously to the three finite element types adopted to model concrete, FRP and steel; each type obeying the proper yield criterion. Large scale prototypes of a few FRP-strengthened RC beams, experimentally tested up to failure, have been numerically analyzed. The reliability and effectiveness of the proposed methodology has then been proved by comparison between experimental and numerical results showing also the capability of predicting, even if qualitatively, the failure mechanism type of the analyzed element.

References

[1] Almusallam T.H. and Al-Salloum Y.A. (2005). Use of glass FRP sheets as external flexure reinforcement in RC beams. Department of Civil Engineering, King Saud University; 1Ű-15.
[2] American Concrete Institute ACI 440.(2008). Guide for the design and construction of externally bonded FRP systems for strengthening concrete structures, ACI 440.2R-08.
[3] Bažant Z.P. (1986). Mechanics of distributed cracking. Appl Mech Rev.; 39: 675–705.
[4] Bresler B and Scordelis AC. (1963). Shear stength of reinforced concrete beams. Journal of American Concrete Institute; 60(1): 51–72.
[5] Chen W.F.(1982). *Plasticity in reinforced concrete,* (McGraw-Hill, USA).
[6] Drucker DC, Prager W.(1952). Soil mechanics and plastic analysis or limit design. Quarterly Applied Mathematics; 10: 157–165.
[7] De Domenico D. RC members strengthened with externally bonded FRP plates: A FE-based limit analysis approach. Composites Part B: Engineering; (submitted to).
[8] De Domenico D., Pisano A.A. and Fuschi P. (2014). A FE-based limit analysis approach for concrete elements reinforced with FRP bars. Composite Structures; 107: 594–603.
[9] FIB Bulletin 14, (2001). Externally bonded FRP reinforcement for RC structures, Task group 9.3, International Federation of Structural Concrete.
[10] Fuschi P. (1999). Structural shakedown for elastic-plastic materials with hardening saturation surface. International Journal of Solids and Structures; 36: 219–240.
[11] Le C.V., Nguyen-Xuan H. and Nguyen-Dang H. (2010). Upper and lower bound limit analysis of plates using FEM and second-order cone programmin. Computers and Structures; 88: 65–73.
[12] Lee J. and Fenves G.L. (1998). Plastic-damage model for cyclic loading of concrete structures. Journal of Engineering Mechanics, ASCE; 124: 892–900.

[13] Li T and Crouch R. (2010). A C_2 plasticity model for structural concrete. Computers and Structures; 88: 1322–1332.
[14] Limam O., Foret G. and Ehrlacher A. (2003). RC two-way slabs strengthened with CFRP strips: experimental study and a limit analysis approach. Composite Structures; 60: 467–471.
[15] Lubliner J., Oliver J., Oller S. and Oñate E. (2010) A plastic-damage model for concrete. Int J of Solids and Structures; 25(3): 299–326.
[16] Mackenzie D and Boyle J.T. (1993). A method of estimating limit loads by iterative elastic analysis, Parts I, II, III. International Journal of Pressure Vessels and Piping; 77: 77–142.
[17] Menétrey, P. and Willam K.J. (1995). A triaxial failure criterion for concrete and its generalization. ACI Structural Journal; 92: 311–318.
[18] Pisano A.A. and Fuschi P. (2007). A numerical approach for limit analysis of orthotropic composite laminates. Int J Numerical Methods Eng.; 70: 71–93.
[19] Pisano A.A., Fuschi P. and De Domenico D. (2012). A layered limit analysis of pinned-joints composite laminates: Numerical versus experimental findings. Composites: Part B; 43: 940-952.
[20] Pisano A. A., Fuschi P. and De Domenico D. (2013a). A kinematic approach for peak load evaluation of concrete elements. Computers and Structures; 119: 125–139.
[21] Pisano A.A., Fuschi P. and De Domenico D. (2013b). Peak load prediction of multi-pin joints FRP laminates by limit analysis. Composite Structures; 96: 763–772.
[22] Pisano A.A., Fuschi P. and De Domenico D. (2013c). Peak loads and failure modes of steel-reinforced concrete beams: predictions by limit analysis. Engineering Structures; 56: 477–488.
[23] Pisano A.A., Fuschi P. and De Domenico D. (2014). Limit state evaluation of steel-reinforced concrete elements by von-Mises and Menétrey-Willam-type yield criteria. International Journal of Applied Mechanics. Imperial College Press; (in press).
[24] Ponter A.R.S and Carter K.F. (199). Limit state solutions, based upon linear elastic solutions with spatially varying elastic modulus. Comput Methods Appl Mech Eng.; 140: 237–258.
[25] Ponter A.R.S, Fuschi P. and Engelhardt M. (2000). Limit analysis for a general class of yield conditions. Eur J Mechanics/A Solids; 19: 401–421.
[26] Prager W.(1959). *An Introduction to Plasticity*. Addison-Wesley: Reading, MA.
[27] Sloan S.W.(1988). Lower bound limit analysis using finite elements and linear programming. Int J Num Anal Methods in Geomechanics; 12: 61–77.
[28] Spiliopoulos K, Weichert D. *Direct Methods for Limit States in Structures and Materials.* Dordrecht: Springer Science+Business Media B.V., 2013.
[29] Tsai S.W. and Wu E.M. (1971). A general theory of strength for anisotropic materials. J. Compos. Mater.; 5: 58–80.
[30] Zhang J., Zhang Z. and Chen C. (2010). Yield criterion in plastic-damage models for concrete; Acta Mechanica Solida Sinica; 23(3): 220–230.